Pairwise interactions in inertially driven one-dimensional microfluidic crystals

Pairwise interactions in inertially driven one-dimensional microfluidic crystals

Kaitlyn Hood[1,*] and Marcus Roper[2]
[1]*Department of Mechanical Engineering, Massachusetts Institute of Technology, Cambridge, Massachusetts 02139, USA*
[2]*Department of Mathematics, University of California Los Angeles, Los Angeles, California 90095, USA*

(Received 3 July 2017; published 5 September 2018)

In microfluidic devices, inertia drives particles to focus on a finite number of inertial focusing streamlines. Particles on the same streamline interact to form one-dimensional microfluidic crystals (or "particle trains"). Here we develop an asymptotic theory to describe the pairwise interactions underlying the formation of a one-dimensional crystal. Surprisingly, we show that particles assemble into stable equilibria, analogous to the motion of a damped spring. The damping of the spring is due to inertial focusing forces, and the spring force arises from the interplay of viscous particle-particle and particle-wall interactions. The equilibrium spacing can be represented by a quadratic function in the particle size and therefore can be controlled by tuning the particle radius.

DOI: 10.1103/PhysRevFluids.3.094201

I. INTRODUCTION

In hydrodynamics, viscosity arises from collisions between the molecules of the fluid, transferring momentum from fast regions to slower regions. As a result, viscosity resists large velocity gradients and is often compared to frictional damping. In contrast, fluid inertia maintains momentum and enhances velocity gradients in the flow. Heuristically, viscosity is thought to impede or dampen flow while inertia is thought to enhance it. Here we present a counterexample to this intuition. The geometry of the proposed system reverses the role of viscosity and inertia, so that viscous stresses perpetuate motion while inertial stresses dampen motion.

We consider the motion of two neutrally buoyant particles suspended in a fluid moving through a rectangular channel. The Reynolds number of the flow is chosen between 1 and 100, so that inertial stresses are equal to or greater than viscous stresses. The fluid inertia causes the particles to migrate across streamlines and focus at finitely many inertial focusing streamlines [1–4]. Experiments [5–9] show that inertially focused particles "crystallize" into trains with regular spacing [Figs. 1(a) and 1(b)].

There are two types of crystallization in rectangular microchannels for consideration: (1) cross-streamline crystals [which can be two-dimensional (2D) or three-dimensional (3D)] shown in Fig. 1(b) and (2) same-streamline crystals [effectively one-dimensional (1D) crystals] shown in Fig. 1(a). Real particle trains are typically made up of a mixture of the two types [8]. Nonetheless, the two types of crystals have been explained by different mechanisms.

In case (1), lattice Boltzman simulations [6] of the streamlines around a single inertially focused particle showed the existence of two vortices on the opposite side of the channel [Fig. 1(c) reproduces these]. It was hypothesized that the centers of these vortices present stable focusing positions for a second particle. A stable crystal forms with particles alternating between streamlines.

*kaitlyn.t.hood@gmail.com

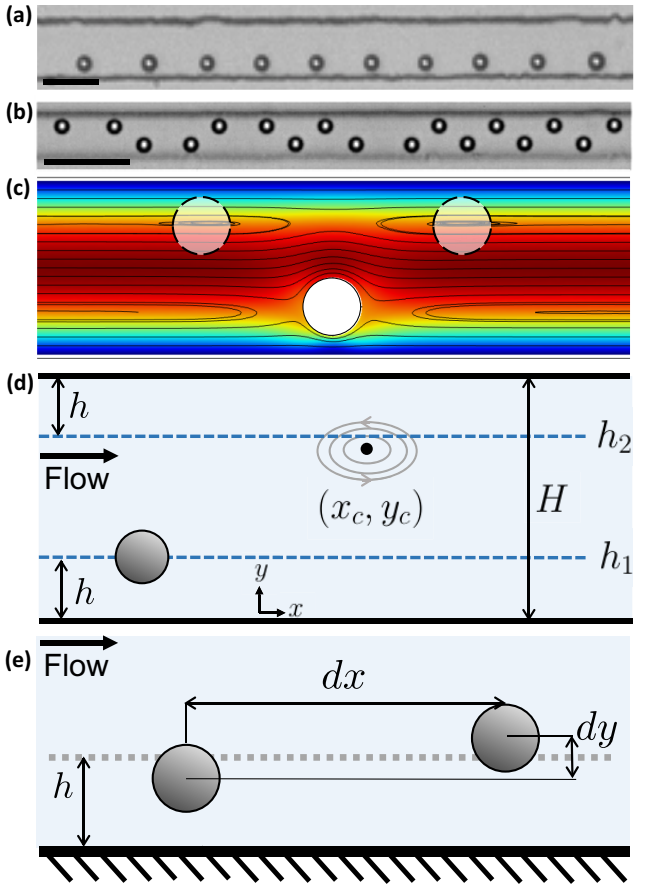

FIG. 1. (a) Particles on the same streamline form a 1D microfluidic crystal for Re = 30 and $\alpha = 0.17$ and $\kappa = 1.7$; scale bar represents 90 μm [8]. (b) Cross-streamline 2D microfluidic crystal; scale bar represents 50 μm [7]. (c) Streamlines around a single inertially focused particle simulated using FEM in Comsol Multiphysics (Los Angeles, CA) show stagnation points on the opposite side of the channel where particles can focus to form a stable crystal with particles alternating between streamlines. (d) Diagram for two particles focusing on opposite streamlines h_1 and h_2. The point (x_c, y_c) (black dot) marks the center of the closed eddy formed by the particle focused at streamline h_1. (e) Diagram for two particles near the inertial focusing streamline and a single wall.

In case (2), crystallization is assumed to occur at the balance of attractive and repulsive interparticle forces. The repulsive forces appear to be symmetric, while the attractive forces appear to be nonsymmetric and therefore are believed to have separate origins [7]. Lee *et al.* hypothesize that the repulsive forces are not due to fluid inertia, but rather are due to viscous interactions with the channel wall pushing the particles away from the focusing streamline. They assert that the attractive force arises from the inertial lift force pushing the particles back to their focusing streamlines and overshooting, creating a harmonic oscillator type potential.

While this mechanism gives a qualitative explanation of crystallization, it remains untested and generates more questions about the dynamics of train formation: What are the magnitudes of the attractive and repulsive forces? How do these forces depend on the experimental parameters? Can we predict the lattice length λ as a function of the experimental parameters? While general trends are well documented, and numerical simulations can predict dynamics for a single device, there is no theoretical model that can predict the lattice length for a general class of devices and range of

parameters. Such a theory could be used to engineer trains with a specific lattice length. Controlling the lattice length is necessary in applications such as high-speed imaging, flow cytometry, and entrapment of live cells in droplets for tissue printing [10,11]. A quantitative theory of lattice formation and equilibrium spacings would be one step towards rational design of such devices.

In order to develop our model, we analyze the interactions of pairs of particles confirming that pairs can form stable doublets in both cross-stream and same-streamline configurations. In the process of deriving the equilibrium spacing length between two particles, we discover that these stable equilibria behave like simple damped spring models where viscosity and inertia play unintuitive roles in the dynamics.

II. CROSS-STREAMLINE PAIRS

First we explore the mechanism by which particles interact across streamlines. We demonstrate mathematically how the center of a closed vortex can become a stable focusing position for a particle. Simulations [6] of the flow around a single inertially focused particle show closed vortices on the opposite side of the channel [reproduced in Fig. 1(c) and verified [12] against drag coefficient measurements by Chow *et al.* [13]].

Consider fluid flowing through a rectangular channel with height H, width W, and aspect ratio $\kappa = W/H$, and fluid flowing with maximum velocity U. If the fluid has density ρ and viscosity μ, then the channel Reynolds number is $\mathrm{Re} = \rho U H/\mu$. We consider two spherical particles with radius a and density ρ suspended in the fluid, both close to a given inertial focusing streamline. The distance h between the inertial focusing streamline and the channel wall depends on the dimensionless particle radius $\alpha = a/H$ [3] and can be predicted from asymptotic theory [14]. Let dx be the downstream separation of the two particles (from center to center) and dy be the vertical displacement of the downstream particle above the upstream particle [Fig. 1(d)].

We assume that the original particle is on the focusing streamline $(y, z) = (h_1, 0)$ and the vortices are near the focusing streamline $(y, z) = (h_2, 0)$. Due to symmetry of the channel and inertial focusing, we will assume all particles are restricted to the plane $z = 0$. Initially we treat the eddies phenomenologically, but we note that the eddies themselves can be quantitatively reproduced using the same model we develop for same streamline interactions [12].

For simplicity, we assume the closed vortex has an elliptical shape in the x, y plane and is centered at (x_c, y_c), where y_c is sufficiently close to h_2. Then we can express the vortex as a second-order system of ordinary differential equations (ODEs):

$$\dot{x} = -\beta^2(y - y_c), \quad \dot{y} = \omega^2(x - x_c)\,. \tag{1}$$

The direction of the eddy is determined by the location of the nearest channel wall. For example, in the case shown in Fig. 1(d), because of the upper channel wall at $y = H$, the local shear flow on the streamline $y = h_2$ will be negative, i.e., $-\gamma(y - h_2)$, where $\gamma > 0$. Therefore, the eddy should have a counterclockwise orientation.

Now we consider a second particle near the h_2 streamline. We adapt the asymptotic theory developed by Hood *et al.* [14,15] for rectangular channels. Since numerical experiments show that viscous stresses dominate momentum flux terms over the entire fluid-filled domain, V, we can perform a regular perturbation expansion in the particle Reynolds number Re_p, treating the viscous and pressure stresses as dominant terms, and the inertial stress as a perturbative correction.

We use the Lorentz reciprocal theorem [16] to represent the inertial lift force $\mathbf{F}_L$ as a volume integral that involves the following three solutions of Stokes equations ($\mathrm{Re}_p = 0$): (1) $\bar{\mathbf{u}}$, the undisturbed flow through the channel, (2) $\mathbf{u}$, the solution for a force-free and torque-free sphere moving through the microchannel, and (3) a test velocity $\hat{\mathbf{u}}$ for the slow ($\mathrm{Re}_p = 0$) movement of a particle in the lateral direction in a quiescent fluid. The total force on a particle that is constrained

from migrating across streamlines can be written as an integral:

$$\mathbf{F}_L = \mathrm{Re}_p \int_V \hat{\mathbf{u}} \cdot (\bar{\mathbf{u}} \cdot \nabla \mathbf{u} + \mathbf{u} \cdot \nabla \bar{\mathbf{u}} + \mathbf{u} \cdot \nabla \mathbf{u})\, dv. \tag{2}$$

To expose the role played by particle size in determining the lift force,we expanded $\mathbf{u}$ and $\hat{\mathbf{u}}$ as a two-term series in $\frac{a}{H}$, the ratio of the particle radius to the channel depth. The lift force $\mathbf{F}_L$ at the point $\mathbf{x}_0$ in the channel can be expressed as a two-term asymptotic expansion with coefficients $\mathbf{c}_4(\mathbf{x}_0)$ and $\mathbf{c}_5(\mathbf{x}_0)$. Specifically,

$$\mathbf{F}_L(\mathbf{x}_0) \sim \frac{\rho U^2 a^4}{H^2}\left[\mathbf{c}_4(\mathbf{x}_0) + \frac{a}{H}\mathbf{c}_5(\mathbf{x}_0)\right]. \tag{3}$$

The coefficients $\mathbf{c}_4(\mathbf{x}_0)$ and $\mathbf{c}_5(\mathbf{x}_0)$ are dimensionless constants including both analytical and numerically computed components and depend on the location of the particle $\mathbf{x}_0$ and the aspect ratio of the rectangular cross section.

To compute the inertial migration velocity in the neighborhood of $y = h_2$, we Taylor expand Eq. (3) around $y = h_2$. As a result, the particle inertial migration velocity can be expressed as $\dot{y} = -\Gamma(y - h_2)$, where

$$\Gamma = \frac{a^3 U \mathrm{Re}}{6\pi H^4}\left(95.9 + 163.4\frac{a}{H}\right). \tag{4}$$

Adding inertial focusing to the system of ODEs in Eq. (1), we arrive at

$$\dot{x} = -\beta^2(y - y_c), \tag{5}$$

$$\dot{y} = \omega^2(x - x_c) - \Gamma(y - h_2)\,. \tag{6}$$

This system of ODEs has an equilibrium solution at (x_*, y_*) where

$$x_* = x_c + \frac{\Gamma}{\omega^2}(y_c - h_2)\,, \quad y_* = y_c\,. \tag{7}$$

We make the change of variables $X = x - x_*$ and $Y = y - y_*$, and then by substitution we can rewrite this as a second-order ODE in Y:

$$\ddot{Y} + \Gamma\dot{Y} + \omega^2\beta^2 Y = 0\,. \tag{8}$$

The right-hand side of Eq. (8) equal to zero if we choose y^* to be

$$y^* = \frac{\omega^2\beta^2 y_c + \Gamma h_2}{\omega^2\beta^2 + \Gamma}\,. \tag{9}$$

Then Eq. (8) becomes a homogeneous second-order differential equation with constant coefficients or a damped harmonic oscillator. We see that the damping term is proportional to Γ, the inertial focusing constant. As a result, the particle focuses to $(X, Y) = (0, 0)$ or $(x, y) = (x_c, y^*)$.

We have shown that the inertially driven damping of particle motion in an eddy forces the particle to focus to a single point. Notice that the focusing position of the particle is not exactly on the inertial-focusing streamline, but at a weighted average between the streamline and the center of the eddy, where the weights are the inertial focusing constant Γ and the elliptical eddy constants β and ω.

This analysis provides a mechanism by which particles can form stable cross-stream pairs. However, it does not appear to apply to same-streamline crystals because there are no closed eddies on the same streamline as the focused particle, only a recirculating flow [Fig. 1(c)]. In order to explain same-streamline crystallization, we need to derive a new model from first principles.

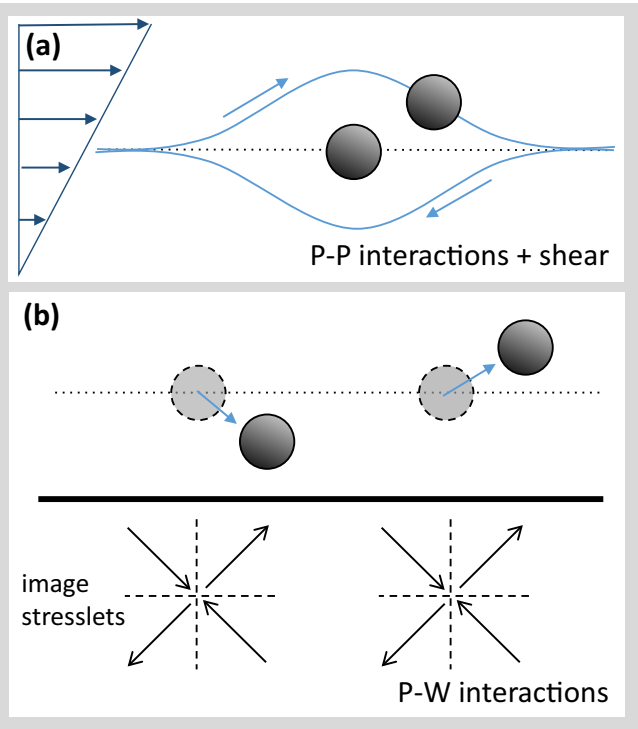

FIG. 2. (a) Viscous P-P interactions in a shear flow predicts "bound" pairs of spheres with closed trajectories [17] and with $\dot{dy} < 0$. Shown in the moving reference frame of one particle. (b) Viscous P-W interactions can be represented by image stresslets. The image on particle 1 acts on particle 2 and vice versa, creating a net $\dot{dy} > 0$.

III. SAME-STREAMLINE PAIRS

Here we derive a model for the assembly of pairs of same-streamline crystals. In order to make an asymptotic expansion, we assume that $a \ll h \ll dx$.

In a rectangular channel flow, numerical experiments show that viscous stresses dominate over momentum flux terms over the entire channel [14]. Hence, a 3D asymptotic analysis of the Navier-Stokes equations for this system showed that a low Reynolds number approximation is valid. This analysis demonstrated that the dominant physics is viscous, and that inertial focusing can be treated as a perturbative effect.

What are the essential ingredients needed to model the interactions of a pair of particles within a same-streamline 1D crystal? First, we need inertial focusing to constrain the particles on a streamline. Second, we need particle-particle (P-P) interactions. Third, we need the local background flow (i.e., the flow in a channel undisturbed by particles), which to first order is a shear flow. Fourth, we find that it is necessary to include particle-wall (P-W) interactions (with the nearest channel wall) in order to achieve a stable configuration. The role of the P-W interactions will be made clear later in this section.

Because the asymptotic theory that accurately predicts the lift force in Eq. (2) arises from a perturbation expansion in small Re_p, we conclude that, in a channel geometry, viscous effects are first order and inertial effects are second order [14]. Therefore, it suffices to approximate the P-P interactions and the P-W interactions with their viscous counterparts. Furthermore, these viscous interactions can be written analytically as a multipole expansion [17,18]. Likewise, inertial focusing

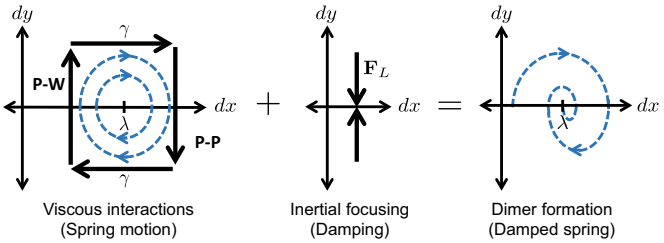

FIG. 3. Analogy between nucleation and damped spring motion.

can be written as a two-term asymptotic series whose coefficients were computed numerically by Hood *et al.* [14].

Viscous P-P interactions in a shear flow results in "bound" pairs of spheres with closed trajectories [17] [Fig. 2(a)]. We will rederive this result using Lamb's solution, the method of reflections, and Faxén's laws in Sec. IV and add additional physics. Because this orbit is clockwise in the sense of the coordinates used in Figs. 1(d) and 2(a), and because we have defined dy to be the vertical displacement between the leading and trailing particle, we observe that $\dot{dy}$ is negative throughout. Starting with the two spheres with $dx \sim 0$, then dy is positive. As the particles orbit, dy decreases monotonically and passes through zero and then becomes negative. The vertical displacement dy reaches its minimum value when $dx = 0$, at which point the trailing particle becomes the leading particle. During this first phase of the orbit, $\dot{dy}$ was negative throughout. In the second phase, after the leading and trailing particles switch, dy starts out positive and decreases monotonically to a negative value, resulting in a negative $\dot{dy}$.

Viscous P-W interactions act in the opposite direction on the vertical displacement dy. We can see this by using the method of images to model the effect of the wall on the particles. To first order, we approximate the image particles by stresslets. The induced velocity on the downstream particle is calculated by evaluating the upstream image stresslet at the center of the downstream particle and has a positive y component. Likewise the induced velocity on the upstream component has a negative y component, so that the net vertical displacement dy is positive [Fig. 2(b)].

The shear flow centered at the height h converts any vertical displacement dy into a streamwise displacement dx. Combining the shear flow with viscous P-P interactions and viscous P-W interactions creates a closed loop with an equilibrium point at $(dx, dy) = (\lambda, 0)$ (Fig. 3 left). In dynamical systems, $(\lambda, 0)$ is called a center and is neutrally stable. Note that when the particles are on the same streamline, neither P-P nor P-W interactions act to alter the spacing dx directly. The equilibrium shows up as a point where $\dot{dy}$ vanishes. Thus, it is not detected using the standard approach to finding equilibria (i.e., analyzing where $\dot{dx} = 0$).

In contrast, inertial focusing acts uniformly on particles, regardless of their separation dx, and always pushes particles back to the inertial focusing streamline at $y = h$. Therefore inertial focusing pushes dy to zero (Fig. 3 center). Adding inertial focusing to the viscous system above creates an asymptotically stable spiral point that converges to $(dx, dy) = (\lambda, 0)$ (Fig. 3 right).

The dynamics of the system of two inertially focused particles interacting mimics the behavior of a damped harmonic oscillator or a spring with frictional damping (Fig. 3). Here the viscous interactions are analogous to the spring motion creating closed trajectories in (dx, dy) space while inertial focusing is analogous to frictional damping. Herein lies the role reversal: viscosity maintains motion (like a spring) and inertia dampens motion (like friction).

IV. DYNAMIC MODEL OF CRYSTALLIZATION

We can make this description rigorous by writing the equations of motion and solving them numerically. Let $\mathbf{x}_i$ for $i = 1, 2$ be the locations of the two particles. We begin by finding the exact solution for the flow around an unbounded parabolic flow around a single force-free and torque-free

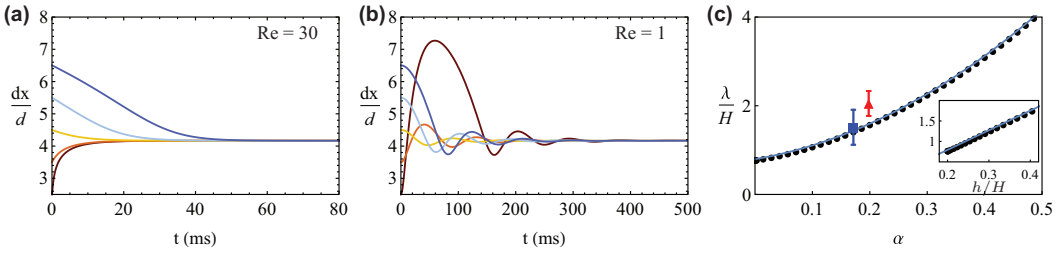

FIG. 4. The separation of two particles $dx(t)$ as a function of time for $a = 6\ \mu$m, different initial separation lengths, and (a) Re $= 30$ or (b) Re $= 1$. (c) The equilibrium separation length λ is a function of the relative particle size $\alpha = a/H$ and Eq. (15) captures this relationship well. Here the markers represent numerical solutions to Eqs. (12)–(13), and the solid line is Eq. (15). Experimental measurements from Kahkeshani *et al.* [8] at $\mathrm{Re}_p = 2.8$ (blue square) and Lee *et al.* [7] (red triangle) agree with our model. Error bars are standard deviations. (Inset) We observe that λ is a linear function of h and can be approximated by Eq. (14).

no-slip sphere. The flow around each particle can be derived using Lamb's solution for the flow exterior to a sphere [19,20]. Here we will keep only the terms that are $O(r^{-2})$ and $O(r^{-3})$. In order to derive the image system in the next step, we must convert Lamb's solution into multipole singularities. In this case the $O(r^{-2})$ term becomes the stresslet $\mathbf{v}^{\mathrm{ST}}$, and the $O(r^{-3})$ term is decomposed into the source dipole $\mathbf{v}^{\mathrm{D}}$ and two stokeslet quadrupoles $\mathbf{v}^{\mathrm{SQ}}$ and $\mathbf{w}^{\mathrm{SQ}}$.

For each particle, we model the viscous wall effects by computing the image system for a plane wall. Blake [21] derived the image system for a stokeslet, and using a similar procedure the image systems for the stresslet $\mathbf{v}^{\mathrm{STim}}$, source dipole $\mathbf{v}^{\mathrm{Dim}}$, and stokeslet quadrupoles $\mathbf{v}^{\mathrm{SQim}}$ and $\mathbf{w}^{\mathrm{SQim}}$ can be derived [12,22,23]. Then the flow around each particle is

$$\mathbf{v}_i \sim \left(\mathbf{v}_i^{\mathrm{ST}} + \mathbf{v}_i^{\mathrm{STim}}\right) + \left(\mathbf{v}_i^{\mathrm{D}} + \mathbf{v}_i^{\mathrm{Dim}}\right) + \left(\mathbf{v}_i^{\mathrm{SQ}} + \mathbf{v}_i^{\mathrm{SQim}}\right) + \left(\mathbf{w}_i^{\mathrm{SQ}} + \mathbf{w}_i^{\mathrm{SQim}}\right). \tag{10}$$

Corrections to v_i from the presence of particle $j \neq i$ are higher order and therefore not included in this step.

Let $\bar{\mathbf{u}}$ be the Poiseuille flow through a rectangular channel [24]. Then, for each particle, we use Faxén's law [20] to compute the induced velocity from the other particle and image system:

$$\mathbf{U}_i = \left(1 + \frac{a^2}{6}\nabla^2\right)(\bar{\mathbf{u}} + \mathbf{v}_j)\Big|_{\mathbf{x}=\mathbf{x}_i}, \quad i \neq j. \tag{11}$$

Here $\mathbf{U}_i = (U_i, V_i, W_i)$. Then we define the relative velocity $d\mathbf{U} = \mathbf{U}_2 - \mathbf{U}_1$.

We again model inertial focusing by Taylor expanding the migration velocity from Hood *et al.* [15] in the coordinate y around h. This gives $\dot{y}_i = -\Gamma(y_i - h)$, where the inertial focusing constant Γ is defined in Eq. (4). Combining the viscous particle interactions $d\mathbf{U} = (dU, dV, 0)$ with the inertial focusing we arrive at a system of ODEs for the dynamics of particle interactions:

$$\dot{dx} = dU, \quad dx(t=0) = k_0 d, \tag{12}$$

$$\dot{y}_i = V_i - \Gamma(y_i - h), \quad y_i(t=0) = h, \quad i = 1, 2. \tag{13}$$

The ODEs depend explicitly on the particle size α, the Reynolds number Re, and the initial separation length $k_0 d$. The equations implicitly depend on the channel aspect ratio κ, but throughout this paper we will consider the same channel as Kahkeshani *et al.* [8], where $W = 60\ \mu$m, $H = 35\ \mu$m, and $\kappa = 1.7$.

Solving ODEs (12)–(13) numerically for $\mathrm{Re} = 30$, $a = 6\ \mu$m, and various initial conditions shows that there is a stable equilibrium length $\lambda = 4.17d$ [Fig. 4(a)]. In contrast, the same system for $\mathrm{Re} = 1$ converges to the same value of $\lambda = 4.17d$, but the harmonic oscillator becomes underdamped

[Fig. 4(b)]. This shows that as Re increases, so does the damping of the spring motion. This behavior is counter to the intuition that viscosity should play the damping role, not the inertia.

How does the lattice length λ scale with experimental parameters? Contrary to expectations, we find that λ does not scale linearly with particle diameter $d = 2a$. From the derivation of our asymptotic model, we would expect λ to depend on both the particle radius a and the distance from the inertial-focusing streamline to the wall h. Surprisingly, we find from the numerical solutions of Eqs. (12) and (13) that λ depends linearly on h [Fig. 4(c) inset]. A polynomial fit of the numerical data predicts that

$$\lambda = -0.2H + 4.8h\,. \tag{14}$$

We conjecture that h is the scaling parameter for the equilibrium spacing, instead of λ. It is not surprising that h influences λ strongly because h appears in the P-W interaction term, which was necessary to include in our model in order to form stable equilibria. In terms of the qualitative model of Lee *et al.* [7], the P-P interactions give rise to a repulsive force between the particles while the P-W interactions lead to an attractive force. Since the strength of the P-W interactions depend explicitly on h, it follows that h should strongly determine the equilibrium spacing λ.

Additionally, h depends implicitly on the relative particle size $\alpha = a/H$ (recall that H is the height of the channel), and can be approximated by a quadratic polynomial [14]. Therefore, we expect that λ can be expressed as a function of the relative particle size α. Using a similar analysis, we observe that for infinitesimal particle sizes, the equilibrium spacing λ approaches a constant $\lambda \sim 0.8H$ [Fig. 4(c)]. As particle size α increases, λ also increases. A polynomial fit of the numerical data for λ predicts that

$$\frac{\lambda}{H} = 0.8 + 2.2\alpha + 9.1\alpha^2\,. \tag{15}$$

We compare the numerical data and the numerical fit in equation (15) to experimental data from Kahkeshani *et al.* [8] (at $\mathrm{Re}_p = 2.8$) and Lee *et al.* [7]. Our model with no fitting parameters (15) matches well with the experimental data [Fig. 4(c)]. This fit persists even though the channels have different aspect ratios ($\kappa = 1.7$ and $\kappa = 3.6$, respectively), suggesting that the modeling assumption that the flow is predominantly 2D is valid.

We note that the equilibrium spacing λ is independent of Re in our theory (though our theory is asymptotically correct as $\mathrm{Re} \to 0$, so higher order corrections are needed to model the effect of Re on the equilibrium spacing). In our model, Re does not impact the equilibrium of the system, only the degree of damping.

V. CRYSTALLIZATION AT MODERATE REYNOLDS NUMBERS

In our model, we assume particle interactions are dominated by viscosity, which is asymptotically correct in the limit of small Reynolds numbers. However, particle train formation still occurs at moderate Re, and preferred spacings of particles can change as Re increases [8].

Kahkeshani *et al.* [8] measured the interparticle spacings of particle trains as the particle Reynolds number Re_p changes. At $\mathrm{Re}_p = 2.8$ they measured a pdf of particle spacings that yielded $\lambda = (4.4 \pm 1.2)d$, which agrees with our theoretical prediction of $\lambda = 4.17d$ in Sec. IV [Fig. 4(c)]. However, at $\mathrm{Re}_p = 8.3$, they measure $\lambda = (2.0 \pm 0.3)d$, which does not agree with our theory. While we expect that our theory is valid only at lower values of Re_p, some insight into train formation at intermediate Re_p can be gleaned from examining particle paths.

As a first step toward a physical theory for crystallization at moderate Reynolds numbers, we adopt an approach recently used to study particle chaining in acoustic streaming flows [25,26]. We analyze the vortical structures created by single particles and then look for patterns of interference between particles. Klotsa *et al.* found empirically that particles tend to organize themselves into configurations that minimize total kinetic energy in the surrounding flow [26].

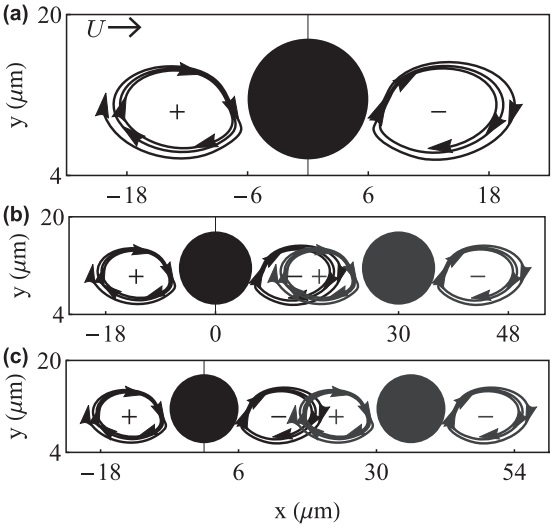

FIG. 5. (a) A particle on the inertial focusing streamline acts on a second particle, drawing vortical path lines both upstream and downstream. The trailing vortex spirals outward while the leading vortex spirals inward. (b) If particles approach too closely, then vortices interfere constructively. (c) If particles are spaced further apart, the vortices interfere destructively.

We investigate the approximate velocity around a single inertially focused particle $\mathbf{U}_i$. Note that the trajectories of $\mathbf{u}_i(\mathbf{x})$ show the paths that another particle would follow if introduced at a point $\mathbf{x}_0 = (x_0, y_0)$; they are therefore particle paths, not streamlines. These particle paths are explained by the schematic in Fig. 3. Specifically, we constrain particle 1 to the streamline $y = h$, then the path of particle 2 $[x(t), y(t)]$ would satisfy

$$\dot{x} = w_x\,, \quad x(0) = x_0, \tag{16}$$

$$\dot{y} = w_y\,, \quad y(0) = y_0, \tag{17}$$

where $\mathbf{w} = (w_x, w_y, w_z)$ satisfies

$$\mathbf{w} = \left(1 + \frac{a^2}{6}\nabla^2\right)\mathbf{v}_1\Big|_{x_1=0, y_1=h}. \tag{18}$$

Notice that $\mathbf{w}$ is the induced flow of particle 2 due to particle 1. It is not $\mathbf{v}_1$, the flow around particle 1, which could be compared directly to the numerical simulation of the flow around an inertially focused particle [Fig. 1(c)]. In our analysis, we consider only one-way interactions, so particle 1 does not leave its inertially focused position.

We observe that the particle paths form a leading vortex and a trailing vortex both with the same sense of rotation [Fig. 5(a)]. On closer observation we notice that neither structure is closed. These zones of recirculation have been observed experimentally [8]. The leading vortex is an inward spiral, while the trailing vortex is an outward spiral (Fig. 5). Closure (or not) of the eddies is not a significant factor in our subsequent analysis.

There is an optimum spacing between the particles that minimizes total kinetic energy. If the particles are brought close enough together, then the vortices overlap and reinforce each other, as shown in Fig. 5(b). No longer canceling, the kinetic energy of the flow will now increase. The orientation of the vortices agree with the pair trajectories computed in Kahkeshani *et al.* [8]. Conversely, when two particles are spaced far apart, their respective leading and trailing vortices will tend to cancel each other, as shown in the schematic in Fig. 5(c). Following the reasoning of Klotsa

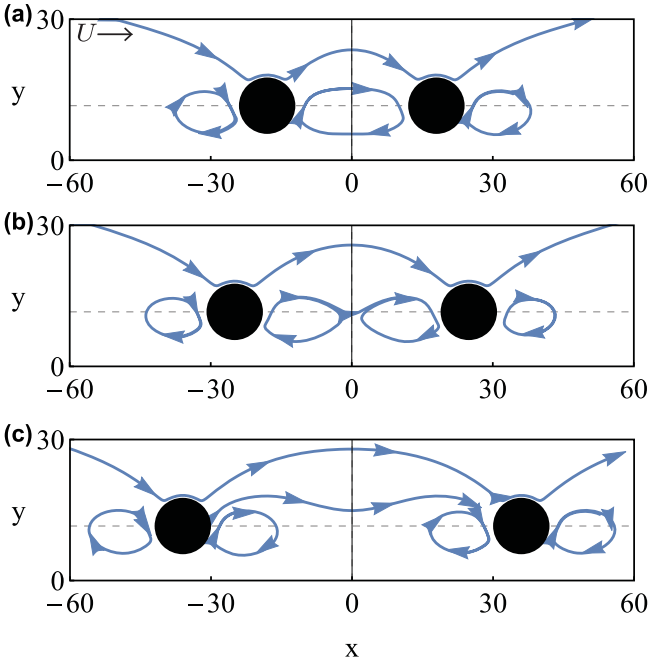

FIG. 6. Vortex interactions for two inertially focused particles. (a) $dx = 3d < \lambda$, (b) $dx = 4.17d = \lambda$, (c) $dx = 6d > \lambda$.

et al. [26], we expect the particles to self-organize into a configuration that minimizes the kinetic energy, i.e., intermediate between Figs. 5(b) and 5(c).

We confirmed that these predictions are supported in our simulations of particles interacting at small Reynolds numbers. We compute particle paths around two inertially focused particles separated by a distance λ, i.e., the particles are located at $(x_1, y_1) = (0, h)$ and $(x_2, y_2) = (dx, h)$. Then the particle paths are determined by Eqs. (16)–(17) where

$$\mathbf{w} = \left(1 + \frac{a^2}{6}\nabla^2\right)(\mathbf{v}_1 + \mathbf{v}_2)\Big|_{x_1=0, x_2=dx, y_1=y_2=h}. \tag{19}$$

The paths determined by Eqs. (16)–(17) and (19) represent the interference of the vortices in Figs. 5(b) and 5(c). When the two particles are close together, $dx < \lambda$, then the two vortices combine to form a closed ring [Fig. 6(a)]. The two vortices overlap and reinforce each other, thereby increasing the total kinetic energy of the system. When the particles are too far apart $dx > \lambda$, the vortices cancel only weakly [Fig. 6(c)]. At the center point of the particles, the paths are clearly unstable. Conversely, when the particles are at their equilibrium spacing $dx = \lambda$, the vortices connect to each other but maintain their distinct centers [Fig. 6(b)]. In this configuration, the vortices cancel at the midpoint creating a third stagnation point, which decreases the total kinetic energy.

As Re_p increases, we expect that the boundary layers on the particles should decrease. According to Kahkeshani *et al.* [8], we would expect that, at some critical Re_p, a new pair of vortices appear closer to the particle in Fig. 5(a). Since the size and location of the vortices determine the equilibrium spacing λ between the particles, we would expect that higher Re_p particle trains should have smaller λ.

VI. CONCLUSIONS

Under our model, pairs of particles organize into stable equilibria that are analogous to damped springs, in which the expected roles of inertia and viscosity have been reversed. Viscous flow maintains harmonic motion, like a spring, while inertial focusing results in a damping effect.

The essential ingredients needed to model the harmonic motion are shear flow, particle-particle interactions, and particle-wall interactions. We showed that particle-wall interactions are necessary to achieve negative vertical displacement dy, and therefore necessary to achieve closed trajectories in the viscous harmonic motion.

We developed an asymptotic model to describe this behavior and produced a formula for the lattice spacing λ. We envisage that the model for particle spacing [12] will be generally useful for reduced order simulations for particles in inertial microfluidic devices. We showed that λ scales with the distance h between the inertial focusing streamline and the channel wall. Since the distance h depends on the relative particle size $\alpha = a/H$, the lattice spacing λ can be tuned by changing particle sizes. As a result, not only is the effect of the channel walls necessary to model the dynamics, but it also sets the scaling for the lattice length.

Additionally, we have shown that both the cross-stream pairs and same-stream pairs form a stable configuration when a closed particle path is combined with inertial focusing to a streamline. In the case of same-stream pairs, the closed particle path is not apparent at the level of the fluid velocity and requires asymptotic approximations to reveal the underlying vortical structure of the system.

ACKNOWLEDGMENTS

This material is based upon work supported by the National Science Foundation under Award No. DMS-1606487 (to K.H.) and DMS-1312543 (to M.R.). This work was partially supported by the UCLA Dissertation Year Fellowship (to K.H.). We thank Lawrence Liu for performing preliminary simulations (supported by DMS-1045536) and Hamed Haddadi and Soroush Kahkeshani for helpful discussions.

[1] G. Segré and A. Silberberg, Radial particle displacements in Poiseuille flow of suspensions, Nature (London) **189**, 209 (1961).

[2] D. Di Carlo, D. Irimia, R. G. Tompkins, and M. Toner, Continuous inertial focusing, ordering, and separation of particles in microchannels, Proc. Natl. Acad. Sci. USA **104**, 18892 (2007).

[3] D. Di Carlo, J. F. Edd, K. J. Humphry, H. A. Stone, and M. Toner, Particle Segregation and Dynamics in Confined Flows, Phys. Rev. Lett. **102**, 094503 (2009).

[4] Y.-S. Choi, K.-W. Seo, and S.-J. Lee, Lateral and cross-lateral focusing of spherical particles in a square microchannel, Lab Chip **11**, 460 (2011).

[5] J.-P. Matas, V. Glezer, É. Guazzelli, and J. F. Morris, Trains of particles in finite-Reynolds-number pipe flow, Phys. Fluids **16**, 4192 (2004).

[6] K. J. Humphry, P. M Kulkarni, D. A. Weitz, J. F. Morris, and H. A. Stone, Axial and lateral particle ordering in finite Reynolds number channel flows, Phys. Fluids **22**, 081703 (2010).

[7] W. Lee, H. Amini, H. A. Stone, and D. Di Carlo, Dynamic self-assembly and control of microfluidic particle crystals, Proc. Natl. Acad. Sci. USA **107**, 22413 (2010).

[8] S. Kahkeshani, H. Haddadi, and D. Di Carlo, Preferred interparticle spacings in trains of particles in inertial microchannel flows, J. Fluid Mech. **786**, R3 (2016).

[9] A. E. Reece and J. Oakey, Long-range forces affecting equilibrium inertial focusing behavior in straight high aspect ratio microfluidic channels, Phys. Fluids **28**, 043303 (2016).

[10] J. F. Edd, D. Di Carlo, K. J. Humphry, S. Köster, D. Irimia, D. A. Weitz, and M. Toner, Controlled encapsulation of single-cells into monodisperse picolitre drops, Lab Chip **8**, 1262 (2008).

[11] H. Amini, A. Jamshidi, T. K. Khurana, F. Mashayekhi, and Y.-S. Wu, Inertial droplet generation and particle encapsulation, US Patent App. 15/347,709 (2017).
[12] See Supplemental Material at http://link.aps.org/supplemental/10.1103/PhysRevFluids.3.094201 for validation of the numerical solver, reproduction of cross-streamline eddies using the model, and detailed derivation of the multipole system and its images.
[13] L. C. Chow, J. E. Leland, J. E. Beam, and E. T. Mahefkey, The drag coefficient of a sphere in a square channel, J. Fluids Eng. **111**, 229 (1989).
[14] K. Hood, S. Lee, and M. Roper, Inertial migration of a rigid sphere in three-dimensional Poiseuille flow, J. Fluid Mech. **765**, 452 (2015).
[15] K. Hood, S. Kahkeshani, D. Di Carlo, and M. Roper, Direct measurement of particle inertial migration in rectangular microchannels, Lab Chip **16**, 2840 (2016).
[16] L. G. Leal, Particle motions in a viscous fluid, Annu. Rev. Fluid Mech. **12**, 435 (1980).
[17] G. K. Batchelor and J. T. Green, The hydrodynamic interaction of two small freely-moving spheres in a linear flow field, J. Fluid Mech. **56**, 375 (1972).
[18] F. R. Da Cunha and E. J. Hinch, Shear-induced dispersion in a dilute suspension of rough spheres, J. Fluid Mech. **309**, 211 (1996).
[19] H. Lamb, *Hydrodynamics* (Dover Publications, New York, 1945).
[20] S. Kim and S. J. Karrila, *Microhydrodynamics: Principles and Selected Applications*, Butterworth-Heinemann Series in Chemical Engineering (Dover Publications, New York, 2005).
[21] J. R. Blake, A note on the image system for a stokeslet in a no-slip boundary, in *Mathematical Proceedings of the Cambridge Philosophical Society* (Cambridge University Press, Cambridge, 1971), Vol. 70, pp. 303–310.
[22] J. R. Blake and A. T. Chwang, Fundamental singularities of viscous flow, J. Eng. Math. **8**, 23 (1974).
[23] S. E. Spagnolie and E. Lauga, Hydrodynamics of self-propulsion near a boundary: Predictions and accuracy of far-field approximations, J. Fluid Mech. **700**, 105 (2012).
[24] T. C. Papanastasiou, G. C. Georgiou, and Andreas N. Alexandrou, *Viscous Fluid Flow* (CRC Press, Boca Raton, FL, 1999).
[25] D. Klotsa, M. R. Swift, R. M. Bowley, and P. J. King, Interaction of spheres in oscillatory fluid flows, Phys. Rev. E **76**, 056314 (2007).
[26] D. Klotsa, M. R. Swift, R. M. Bowley, and P. J. King, Chain formation of spheres in oscillatory fluid flows, Phys. Rev. E **79**, 021302 (2009).